Photochromism and Size Effect of WO_3 and WO_3−TiO_2 Aqueous Sol

Yuping He, Zhenyu Wu, Limin Fu, Chaorong Li, Yanming Miao, Li Cao, Haiming Fan, and Bingsuo Zou*

Nanoscale Physics and Device Laboratory, Institute of Physics, Chinese Academy of Sciences, Beijing 100080, China

Received March 4, 2003. Revised Manuscript Received July 3, 2003

The chromism of tungsten oxides has been investigated for a long time because of its academic and application importance. In this article the photochromism and its dynamics for a WO_3 aqueous sol and WO_3−TiO_2 mixed sols are studied in detail. The chromic performance of the WO_3 aqueous sol is improved significantly by adding TiO_2 aqueous sol, and shows a clear size effect. The intrinsic absorption peak at around 777 nm from W^{5+} in WO_3 nanocluster, which generally appears at around 1000 nm in a WO_3 film, shifts with cluster size because of the quantum confinement effect of delocalized carriers in WO_3 nanoclusters. Besides the 777 nm band from W^{5+} in WO_3, a new extrinsic 640 nm band, due to the transient formation of $WOCl_x$ species in a WO_3 sol in the presence of Cl^- and TiO_2 nanoclusters, appears after adding TiO_2 sol. These results are helpful to the understanding of the chromism of tungsten oxides.

Introduction

WO_3 is one of the important chromogenics that can be continuously switched between two optical states, and which shows many potential applications such as "smart windows", large area displays, automatic glare control in automotive rear-view mirrors, and erasable optical storage, etc., so extensive research[1−5] studies have been carried out since Deb[6] first reported its coloration phenomena at room temperature. Thereafter a lot of work has focused on its variable electronic structures.

It is well established[7] that WO_3 has a defect perovskite-like ReO_3 structure with distorted corner-sharing WO_6 octahedra. Each W ion is octahedrally surrounded by six oxygen ions, and each oxygen ion is linearly flanked by two W ions. As a consequence of this arrangement, the W5*d* level is split into e_g and t_{2g} levels, as shown on the left side of Figure 1. The splitting arises because the e_g orbitals point directly at the electronegative O, whereas the t_{2g} orbitals point away from the nearest neighbors into empty space and are hence lower in energy. Similarly, the O2*p* orbitals are split as indicated in the right part of Figure 1. The $2p_\sigma$ orbitals point directly at the nearest electropositive W ions whereas the $2p_\pi$ orbitals point into empty space. The W5*d* orbitals and the O2*p* orbitals are strongly hybrid-

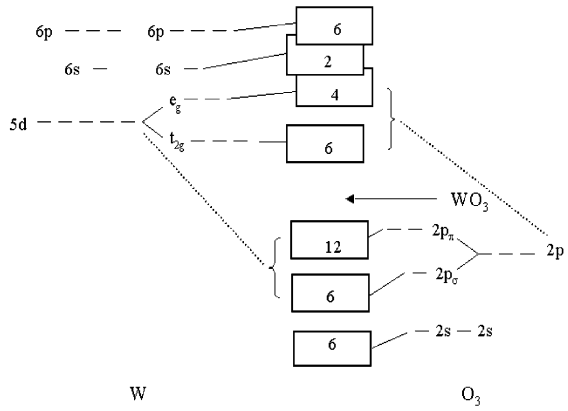

Figure 1. Schematic band structure for the WO_3 defect perovskite-like structure.

ized and correlated with each other, and thus the e_g and t_{2g} levels are partially delocalized.

The number of d electron states available for electron occupancy is finite for each band. For example, the t_{2g} band allows for 6 electrons (with spin degeneracy), and the $2p_\pi$ band allows for 12 electrons (with spin and electron degeneracy). The numbers in the respective bands in Figure 1 indicate the pertinent electron occupancies. WO_3 has 24 electrons in the shown bands of O2p and O2s. The conduction band mainly is made up of the empty W5d and W6sp orbitals. The Fermi energy lies in the gap between the t_{2g} band and the $2p_\pi$ band. The band gap is wide enough to render it transparent.[7] When electrons are added, the excess electrons must occupy the t_{2g} band to lead to W^{5+}, and WO_3, in principle, transforms from transparency to a colored state because of the d−d transition. When the electrons and the related ions are removed from the t_{2g}, WO_3 recovers its original transparent state.

(1) Schigesato, Y. *Jpn. J. Appl. Phys.* **1991**, *30*, 1457.
(2) Bechinger, C.; Oefinger, G.; Herminghaus, S.; Leiderer, P. *J. Appl. Phys.* **1993**, *74*, 4527.
(3) Bechinger, C.; Wirth, E.; Leiderer, P. *Appl. Phys. Lett.* **1996**, *68*, 2834.
(4) Zhang, J. G.; Benson, D. K.; Tracy, C. E.; Deb, S. K.; Czanderna, A. W.; Bechinger, C. *J. Electrochem. Soc.* **1997**, *144*, 2022.
(5) He, T.; Ma, Y.; Cao, Y. A.; Yang, W. S.; Yao, J. N. *Phys. Chem. Chem. Phys.* **2002**, *4*, 1637.
(6) Deb, S. K. *Philos. Mag.* **1973**, *27*, 801.
(7) Granqvist, C. G. *Mater. Sci. Eng. A* **1993**, *168*, 209.

10.1021/cm034116g CCC: $25.00 © 2003 American Chemical Society
Published on Web 09/18/2003

In other words, the photochromic performance of WO_3 is intimately related to the optically excited electron−hole pairs. When WO_3 is irradiated with UV-light, electrons are excited to the conduction band, leaving a hole in the valence band. The photogenerated hole (h^+) can weaken the H−O bond of adsorbed water molecules and cause the water molecules to decompose into protons and highly reactive oxygen radicals,[2,4] i.e.,

$$2h^+ + H_2O \rightarrow 2H^+ + O \quad (1)$$

The oxygen radicals may bind to each other to escape into the ambient media in molecular form; after that, the separated protons (H^+) will break some of the W═O bonds and combine with O^{2-} to form H_2O with the help of photon energy. As a result, this produces colored W^{5+} states in WO_3. Thus, the photochromic reaction in $WO_3 \cdot nH_2O$ can be expressed as[4]

$$WO_3 \cdot nH_2O \xrightarrow{h\nu} WO_3 \cdot (n - x/2)H_2O + xH^+ + xe^- + (x/4)O_2\uparrow$$

$$\xrightarrow{h\nu} W^{6+}_{1-x} W^{5+}_{x} O_{3-x/2} \cdot nH_2O + (x/4)O_2\uparrow \quad (2)$$

Therefore, the recombination of photogenerated carriers (eq 3) is detrimental to the photochromic performance.

$$h^+ + e^- \rightarrow heat \quad (3)$$

TiO_2 has been proven to be an excellent photocatalyst. A lot of investigations have focused on the improvement of TiO_2 photocatalysis. The efficiency of a photocatalytic reaction is improved in a heterogeneous semiconductor system because fast transfer of the photogenerated charges between different types of semiconductor particles suppresses the direct recombination of the photogenerated carriers. One of the heterogeneous semiconductor systems, TiO_2−WO_3, has been investigated for its photocatalytic reactions.[8−12] Thus far the coloration of this composite system has been little studied,[13] especially the relationship between its photocatalysis and coloration and the microscopic mechanism for the improved coloration of WO_3 by TiO_2.

The band gaps of TiO_2 and WO_3 nanoclusters are all in the ultraviolet, and TiO_2 has slightly larger band gap than WO_3. Both the top of the valence band and the bottom of the conduction band of WO_3 are lower than those of TiO_2 (as indicated in Figure 2). WO_3 and TiO_2 can both be excited by UV-light. The photogenerated holes can transfer from the WO_3 valence band to the TiO_2 valence band and the photogenerated electrons can transfer from the TiO_2 conduction band to the WO_3 conduction band. As a result, the photogenerated carriers can be effectively separated and result in improved coloration performance because W^{6+} can be easily reduced to W^{5+}. From another perspective, previous studies of WO_3 photochromism have mainly focused on its film or bulk states, so the quantum size effect in nanoclusters, where highly efficient optical excitation and interfacial charge transfer may contribute to the chromism of the WO_3 system, has been omitted in those studies.

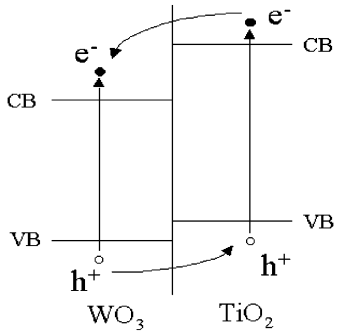

Figure 2. Energy diagram for the WO_3−TiO_2 composite system.

In this paper, the photochromism and its dynamics for the WO_3 aqueous sol and WO_3−TiO_2 sols with different molar ratios and pH values were studied carefully. The photochromic performance of the WO_3 nanoclusters is improved significantly by adding TiO_2 nanoclusters. Their photochromic behaviors show a clear size effect. Besides the intrinsic peak at around 777 nm resulting from W^{5+} in the WO_3 sol, which generally occurs in the range of 900−1100 nm for WO_3 films, a new extrinsic band at around 640 nm appears after adding TiO_2 nanoclusters.

Experimental Section

Preparation of Samples. $Na_2WO_4 \cdot 2H_2O$, HCl, and $TiCl_4$ (Analytical Reagent, from Chemical Reagent Company in Beijing), and dialytic membranes with 12 000−14 000 dialytic modulus, and doubly distilled water were used to prepare TiO_2 and WO_3 sols.

Hydrochloric acid (12 mL, 0.7 M) was added drop by drop to a Na_2WO_4 solution (150 mL, 0.027 M) under magnetic stirring. A transparent aqueous sol was obtained, which was then closed in a dialytic membrane pipe and dialyzed in a 1000-mL beaker containing deionized water for a period of 8 h. The deionized water was periodically replaced until Cl^- ions could not be detected by $AgNO_3$ solution titration. A final transparent sol (pH 4.8, 0.023 M WO_3) was thereby achieved.

$TiCl_4$ (0.4 mL) was added carefully to stirring hydrochloric acid (50 mL, 1 M). A transparent aqueous solution was obtained and dialyzed in the same way as described above. During the dialysis and/or hydrolysis, the solution changed to the sol. In this way, two kinds of final transparent sols (pH 3.5 and 3.0) of 0.063 M TiO_2 containing Cl^- ions were achieved.

A TiO_2 sol (0.063 M) of suitable volume was added drop by drop to the 0.023 M WO_3 aqueous sol under stirring at the WO_3/TiO_2 molar ratios of 4:1, 2:1, 1:1, 1:2, and 1:4x. These samples (including WO_3, TiO_2 sols, and mixtures of different WO_3/TiO_2 molar ratios) using TiO_2 sol at pH 3.5 and 3.0 were denoted as series A and B, respectively. Furthermore, WO_3/TiO_2 samples of 4:1, 2:1, 1:1, 1:2, and 1:4 molar ratios were denoted as A41, A21, A11, A12, A14, B41, B21, B11, B12, and B14, as indicated in Table 1.

Measurements. The morphology of the samples was observed using a CM12 transmission electron microscope (TEM).

The optical absorptions of series A and B samples were thoroughly studied without and with irradiation using a 250-W high-pressure mercury lamp for different time spans in air.

(8) Kwon, Y. T.; Song, K. Y.; Lee, W. I.; Choi, G. J.; Do, Y. R. *J. Catal.* **2000**, *191*, 192.
(9) Song, K. Y.; Park, M. K.; Kwon, Y. T.; Lee, H. W.; Chung, W. J.; Lee, W. I. *Chem. Mater.* **2001**, *13*, 2349.
(10) Li, X. Z.; Li, F. B.; Yang, C. L.; Ge, W. K. *J. Photochem. Photobiol. A: Chem.* **2001**, *141*, 209.
(11) Miyauchi, M.; Nakajima, A.; Watanabe, T.; Hashimoto, K. *Chem. Mater.* **2002**, *14*, 4714−4720.
(12) Li, F. B.; Li, X. J.; Li, X. Z.; Hou, M. F.; Wang, L. Y. *Trans. Nonferrous Met. Soc. China* **2002**, *12*, 707.
(13) Bechinger, C.; Ferrere, S.; Zaban, A.; Sprague, J.; Gregg, B. A. *Nature* **1996**, *383*, 608.

Table 1. Denomination of the Prepared Samples[a]

	sample	
WO_3/TiO_2 (in molar)	TiO_2 (pH 3.5)	TiO_2 (pH 3.0)
4:1	A41	B41
2:1	A21	B21
1:1	A11	B11
1:2	A12	B12
1:4	A14	B14

[a] WO_3 Concentration = 0.023 M, pH = 4.8. TiO_2 Concentration = 0.063 M.

The absorption spectra in the range of 300−900 nm were measured with a TU-1901 UV−visible spectrophotometer.

Results and Discussion

Figure 3 shows the bright-field TEM images of typical samples of series A, and WO_3 (a) and TiO_2 (b); they are all made up of nanoclusters of several nanometers in size. Once they are mixed, aggregation and agglomeration between WO_3 and TiO_2 nanoclusters occur, as indicated in Figure 3(c), where the sizes of the observed particles are much larger than that of their components, and many particles seem to be aggregated or agglomerated and cannot be distinguished separately.

Figure 4 shows the absorption spectra of the series A samples before UV-light irradiation. It is clear that the absorption band edge of the TiO_2 sol is larger than that of the WO_3 sol. With regard to the relationship between the absorption coefficient α and the incident photon energy $h\upsilon$ near the band edge, one can write out a good approximation.[14]

$$\alpha h\upsilon \propto (h\upsilon - E_G)^{n/2} \tag{4}$$

For crystalline samples the value of n depends on whether the interband transition is direct ($n = 1$) or indirect ($n = 4$) or direct forbidden ($n = 3$). For samples in the aqueous sol, that is, amorphous WO_3 and TiO_2, the absorption coefficient α is known to obey eq 4 with $n = 4$ [15] and $n = 3$, respectively. Therefore, the band edges (E_G) of WO_3 and TiO_2 sol can be determined from the corresponding absorption curves as 3.20 eV and 3.48 eV. Both of them are higher than the bulk band gaps of WO_3 (2.80 eV) and TiO_2 (3.20 eV). These results are in good agreement with the predictions of the quantum size effect, which means that E_G shifts to higher energy when the mean size of the nanoclusters decreases.

From Figure 4, the absorption coefficients below the band edge gradually increase with adding more and more TiO_2 nanoclusters, as compared with the original WO_3 aqueous sol, but the band edge does not shift. This phenomenon is related to the interfacial charge neutralization, that is, the negative charges on the surface of WO_3 nanoclusters [16] and the positive charges on the surface of TiO_2 nanoclusters [17] will neutralize when they are mixed. The charge-transfer complexes form due to the binding of the WO_3 and TiO_2 nanoclusters by

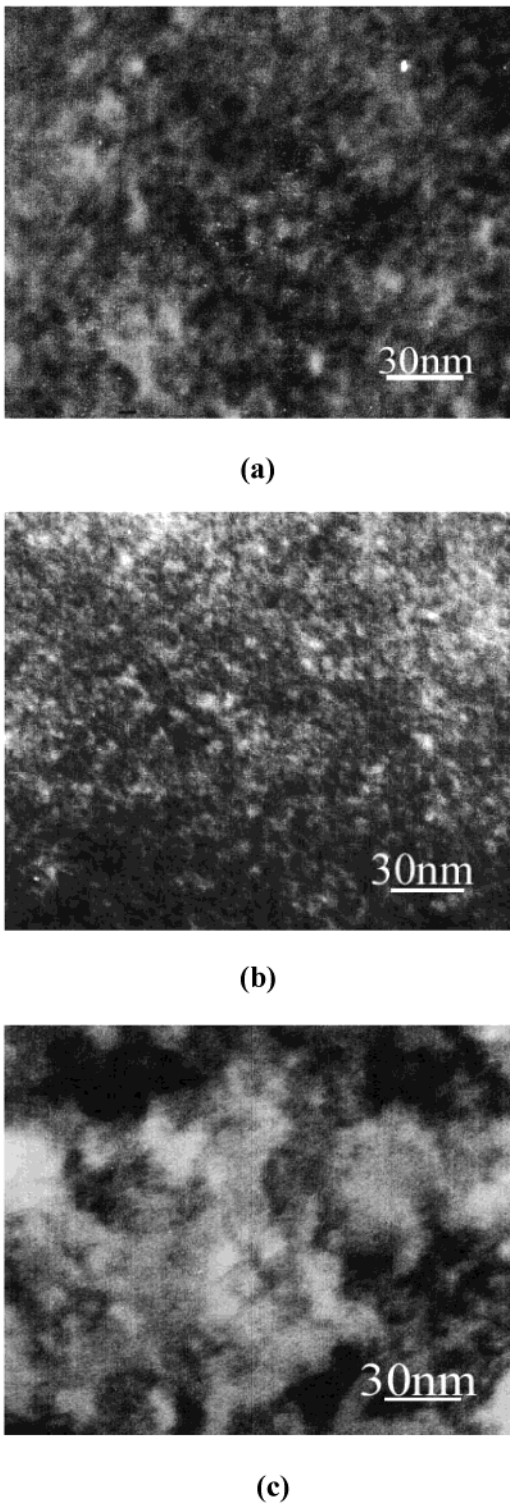

Figure 3. Transmission electron micrographs of series A samples for (a) WO_3; (b) TiO_2; and (c) A21.

Coulomb interactions and thus leads to charge-transfer band tail at the band edge of WO_3. This can be confirmed by the TEM images. With increasing TiO_2 amount, more particle aggregation and agglomeration brings about a stronger charge-transfer band tail absorption below the band edge. However, the band gap of this mixed WO_3 sol did not decrease before irradiation, because the WO_3 cluster aggregation will lead to the red-shift of the band edge. Hence the above aggregation after mixing may occur only for the TiO_2

(14) Johnson, E. J. In *Semiconductors and Semimetals, Vol. 3*; Willardson, R. K., Beer, A. C., Eds.; Academic Press: New York, 1967; Chapter 6.
(15) Kitao, M.; Yamada, S.; Yoshida, S.; Akram, H.; Urabe, K. *Sol. Energy Mater. Sol. Cells* **1992**, *25*, 241.
(16) Hüllen, A. *Angew. Chem.* **1964**, *76*, 588.
(17) Serpone, N.; Lawless, D.; Khairutdinov, R. *J. Phys. Chem.* **1995**, *99*, 16646.

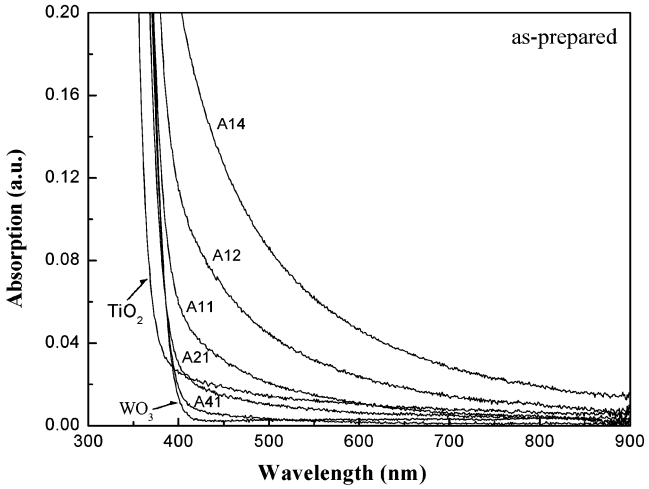

Figure 4. Absorption spectra for the series A samples before UV-light irradiation.

nanoclusters on the surface of each WO_3 nanocluster, not the WO_3 cluster aggregation.

The coloration and bleaching processes for the series A samples were investigated in detail. In fact, during UV light irradiation, the coloration and bleaching processes in the WO_3 sol occur simultaneously. In the coloration process, the photogenerated electrons can accumulate in the WO_3 nanoclusters and participate in the formation of the colored W^{5+} state. In the bleaching process, the electrons, either photogenerated or extracted from the reversal of eq 2, can be removed by reacting with O_2 dissolved in water, as in eqs 5, 6, or 7:

$$O_2 + 4H^+ + 4e^- \rightarrow 2H_2O \quad (5)$$

$$O_2 + 2H^+ + 2e^- \rightarrow H_2O_2 \quad (6)$$

$$O_2 + e^- \rightarrow O_2^- \quad (7)$$

Figure 5(a) is the absorption spectrum of a WO_3 sol just after a 30-min irradiation. The sol shows a blue color and the absorption maximum is around 777 nm, which originates from the $d-d$ transition of W^{5+} in WO_3.[7] Compared with the same $d-d$ transition occurrence at around 1000 nm in WO_3 film, this band significantly blueshifts to 777 nm in sol. This shift is in agreement with the prediction of quantum confinement effect. The W^{5+} related carriers in WO_3 are weakly delocalized, not localized,[18] because the localized carriers did not show a quantum confinement effect. That proves the strong hybridization of the W5*d* orbitals with the O2*p* orbitals.

Figure 5(b) shows the absorption intensity of series A samples at 777 nm just after UV-light irradiation as a function of irradiation time. Adding TiO_2 sol remarkably magnifies the coloration absorption of the WO_3 aqueous sol. First, the irradiation time for the onset of coloration is much shorter than that for the WO_3 sol. This is determined by the competition of the coloration and bleaching processes, i.e., where the coloration dominates over the bleaching early. Second, the coloration rate and efficiency both increase. Furthermore, coloration saturation appears easily in samples A21 and

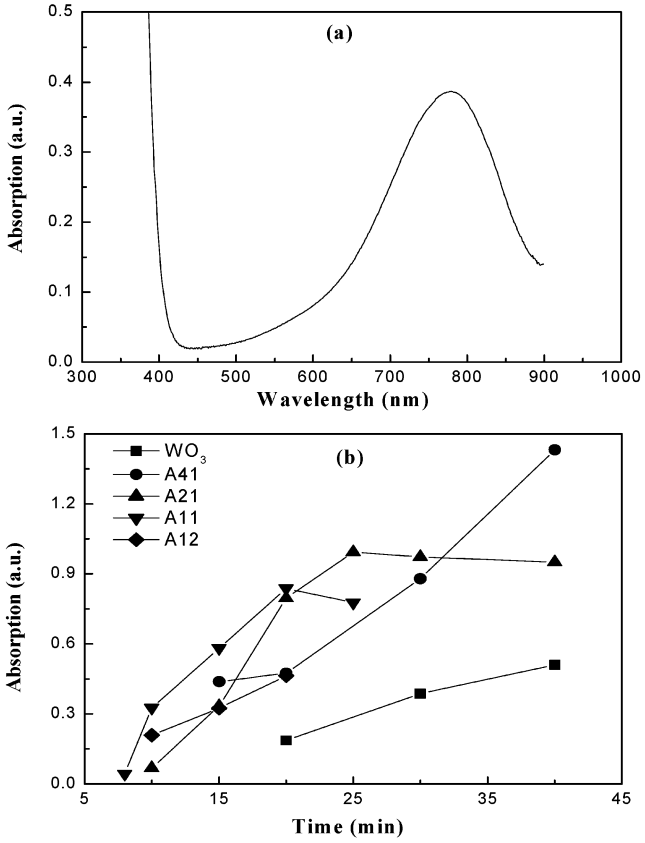

Figure 5. (a) Absorption spectrum of a WO_3 sol just after irradiation for 30 min and (b) absorption intensity vs irradiation time of the 777 nm band just after UV-light irradiation for series A samples.

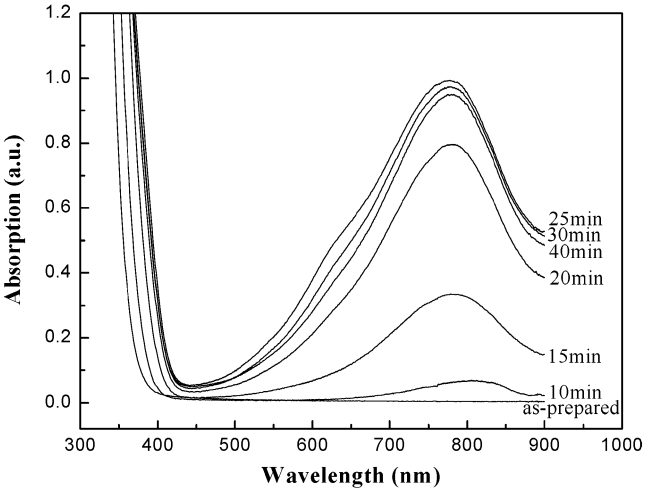

Figure 6. Absorption spectra of sample A21 before and just after UV-light irradiation for different time lengths.

A11 and the corresponding saturation times are 25 min and 20 min, respectively, which are much shorter than that of the WO_3 sol (50 min). The coloration saturation and the difference in saturation coloration time reflect their different photochromic mechanisms. The photochromic behavior of WO_3 is influenced by many factors, such as concentration, composition of chromogenics, and irradiations.

Figure 6 shows the absorption spectra of sample A21 in the range of 300−900 nm for different irradiation times. A shoulder at around 640 nm appears clearly in the curve of 25 min irradiation.

(18) Goodenough, J. B. *Prog. Solid State Chem.* **1971**, *5*, 145.

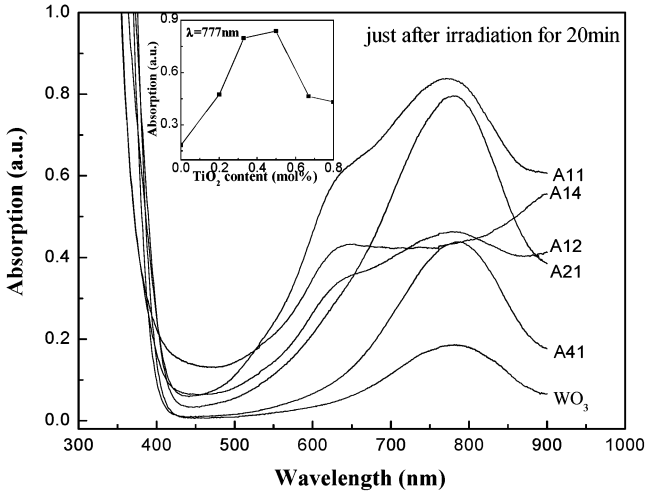

Figure 7. Absorption spectra of the series A samples just after UV-light irradiation for 20 min.

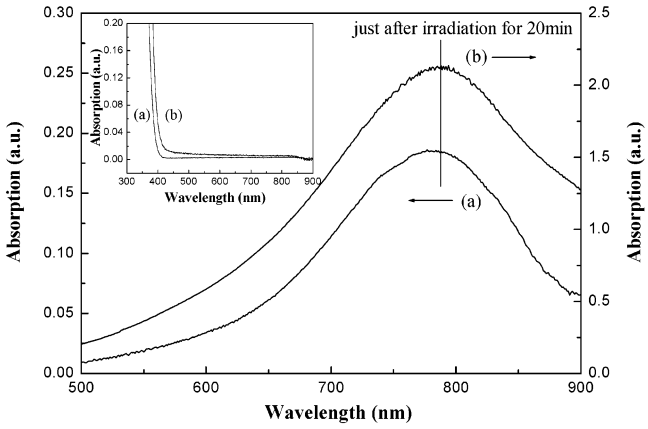

Figure 8. Absorption spectra of WO_3 aqueous sol with concentration (a) 0.023 M and (b) 0.125 M before (in the inset) and just after UV-light irradiation for 20 min.

Figure 7 shows the absorption spectra of series A samples just after UV-light irradiation for 20 min. The intrinsic absorption peak at around 777 nm, due to the $d-d$ transition of W^{5+} in WO_3, is observed in all samples but A14. The peak blueshifts as compared with the results of various WO_3 films obtained by Deb (910 nm),[6] Schirmer et al. (1000 nm),[19] Chemseddine et al. (1240 nm),[20] Schigesato (900−1000 nm),[1] and so on. The shift magnitudes with the WO_3 size come from the contribution of the quantum confinement effect of delocalized carriers.[18]

To confirm the quantum confinement effect, another WO_3 aqueous sol with a higher concentration 0.125 M was prepared and investigated. Figure 8 presents the results of two WO_3 aqueous sols before (indicated in the inset) and just after UV-light irradiation for 20 min. From the inset, one can see that the band edge of the WO_3 sol with a lower concentration (0.023 M) is higher than that of higher concentration (0.125 M); that is, the cluster size of the former is smaller than that of the latter. After coloration, the absorption peak of the former is around 777 nm, and the latter is around 788 nm. This also indicates that the $d-d$ transition and charge-transfer band edge of the WO_3 both blueshift with decreasing size. This result also proves the delocalization nature of the W^{5+} charge in WO_3.

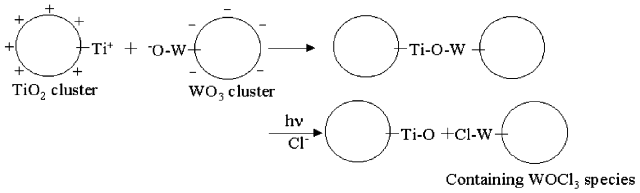

Figure 9. Schematic diagram of the mixing of TiO_2 and WO_3 sols and the formation of $WOCl_3$ species.

With an increasing amount of TiO_2 nanoclusters, the optical density of the 777 nm peak initially increases and subsequently decreases, which is indicated in the inset of Figure 7. With increasing TiO_2, the absorption intensities of the mixed sols increase from 0.19 of WO_3, 0.44 of A41, 0.80 of A21, to 0.84 of A11. However, with further increasing TiO_2, the absorption intensities decrease from 0.84 of A11, 0.46 of A12, to 0.44 of A14. Moreover, for the molar ratio of $TiO_2/WO_3 \geq 1$, a new extrinsic absorption peak at around 640 nm shows up distinctly. Without WO_3 or TiO_2, this peak cannot show up after UV light irradiation. To our knowledge, this peak has never been reported in this chromogenic system before.

To explore the origin of this new peak, we have referred to many papers and textbooks on tungsten compounds. $WOCl_3$ is the only compound with a 640 nm absorption band in this case.[21] Concerning our photochromic system, we have a WO_3 aqueous sol and an acidic TiO_2 sol containing Cl^- on its surface. The WO_3 nanoclusters having negative surface charges interact with TiO_2 nanoclusters having positive surface charges and hence produce a complex with W−O−Ti bonds between them. The TiO_2 nanocluster is a good photocatalyst with redox ability,[22] and thus we believe that the W−O bond in the W−O−Ti bond will break and the Cl^- ions nearby will participate in the photochemical reaction due to the higher reduction ability of Cl^- vs O^{2-}, leading to the formation of $WOCl_x$ species under the UV-light irradiation. This process is shown in Figure 9. To confirm this viewpoint, the photochromic trend of the WO_3 sol caused by adding the TiO_2 sols with different amounts or pH values will be discussed in detail in the next section.

Figure 7 shows that the relative absorption intensity of the 640 nm band is enhanced as contrasted with that at 777 nm with increasing TiO_2, because the concentration of Cl^- ions in the sample increases with increasing the amount of TiO_2 sol. However, it is not necessary to analyze the absolute absorption, as it is also intimately related to the total amount of WO_3. For comparison, another TiO_2 sol (pH 3.0 but the same concentration) was used to mix with the WO_3 sol. Apparently, the lower the pH value of the TiO_2 sol, the more the amount of Cl^- ions and the smaller the mean size of the TiO_2 nanocluster, which is supported by its larger optical band gap of 3.57 eV (pH 3.0) than 3.48 eV (pH 3.5).

(19) Schirmer, O. F.; Wittwer, V.; Baur, G.; Brandt, G. *J. Electrochem. Soc.: Solid-State Sci. Technol.* **1977**, *124*, 749.
(20) Chemseddine, A.; Morineau, R.; Livage, J. *Solid State Ionics* **1983**, *9&10*, 357.
(21) Shen, P. W.; Che, Y. X.; Luo, Y. J. *Inorganic Chemistry Series, Vol. 8;* Science Press: Beijing, 1998; p 539.
(22) Tatsuma, T.; Saitoh, S.; Ohko, Y.; Fujishima, A. *Chem. Mater.* **2001**, *13*, 2838.

Table 2. Optical Parameters Obtained by Three-Peak Gaussian Fitting for A21 and B21 Samples

sample	peak	peak area [a.u.]	peak center [nm]	peak width [nm]	peak height [a.u.]	*A1/A2*
A21 (25 min)	1	78.6	655.6	150.6	0.42	0.58
	2	135.1	784.9	130.7	0.82	
	3	153.0	1012.1	172.0	0.71	
B21 (10 min)	1	145.6	644.1	135.9	0.86	1.47
	2	99.2	771.8	112.8	0.70	
	3	169.9	917.4	162.6	0.83	
B21 (15 min)	1	284.3	644.8	131.3	1.73	1.82
	2	156.1	769.4	103.9	1.20	
	3	239.4	896.4	142.4	1.34	

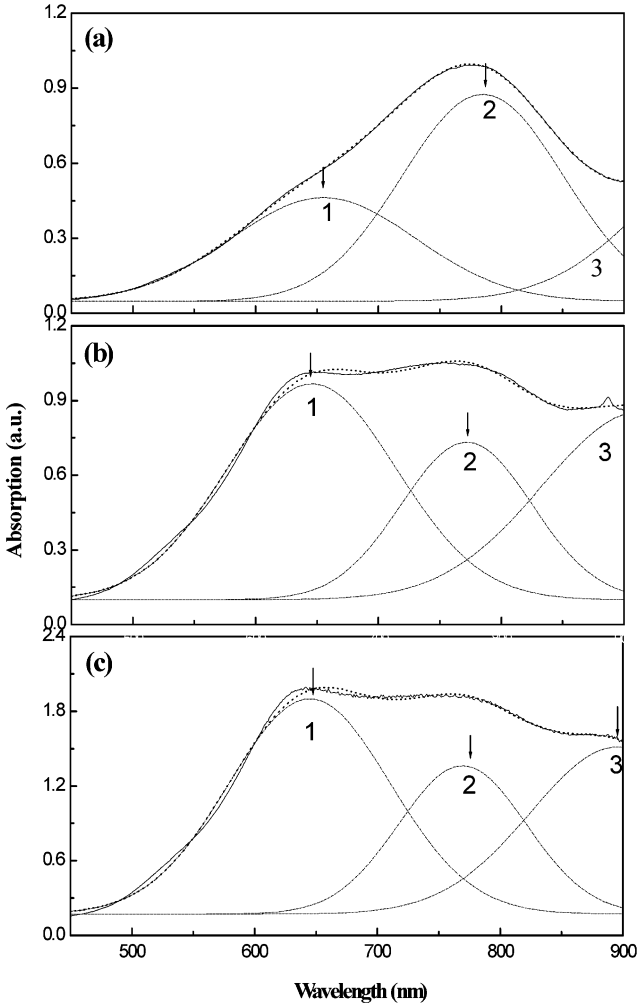

Figure 10. Absorption spectra just after UV-light irradiation for (a) 25 min on sample A21; (b) 10 min and (c) 15 min on sample B21.

Moreover, the lower the pH value of the TiO_2 sol, the stronger the peak at around 640 nm is. The absorption spectra of sample A21 just after irradiation for 25 min and B21 just after irradiation for 10 min and 15 min are presented in Figure 10, where the solid curves denote the experimental data, and the dot and dash−dot curves denote the total and individual three-peak Gaussian fitting results, respectively. On the whole, these fittings work well for the experimental data. Table 2 presents the specific parameters obtained by the fittings.

From Figure 10 and Table 2, the following can be seen. (1) All of the three peaks (655.6, 784.9, and 1012.1 nm) of sample A21 mixed with TiO_2 sol (pH 3.5, larger cluster size) red-shift as compared with that of sample B21 (644.1, 771.8, and 917.4 nm for 10 min irradiation; 644.8, 769.4, and 896.4 nm for 15 min irradiation), which is also due to the quantum size effect. (2) The total absorption intensity or peak area of sample B21 irradiated for 10 or 15 min is far larger than that of sample A21 irradiated for 25 min. That is to say, the coloration rate and the efficiency of the former are higher than that of the latter. Obviously, the smaller the mean size of the nanocluster, the bigger the specific surface area is, and thus the more the contact area and catalytic effect between WO_3 and TiO_2 are, and presumably the more W^{5+}-related states there occur. (3) The area ratio A_1/A_2 of the peak 1 (640 nm, $WOCl_3$) to peak 2 (777 nm, W^{5+}) of sample B21 (1.47 for 10 min irradiation and 1.82 for 15 min irradiation) is much larger than that of sample A21 (0.58). For the same WO_3/TiO_2 molar ratio 2:1 and the same concentration, the net amount of Cl^- ions for the pH 3.0 TiO_2 sol is larger than that of the pH 3.5 sol, which can account for a relatively higher amount of $WOCl_x$ formation. This deduction is in excellent agreement with the above experimental results. (4) With variable irradiation time, the area ratio changes shown in Table 2 indicate the formation of W^{5+} prior to $WOCl_x$. This viewpoint is also supported by the results shown in Figure 6.

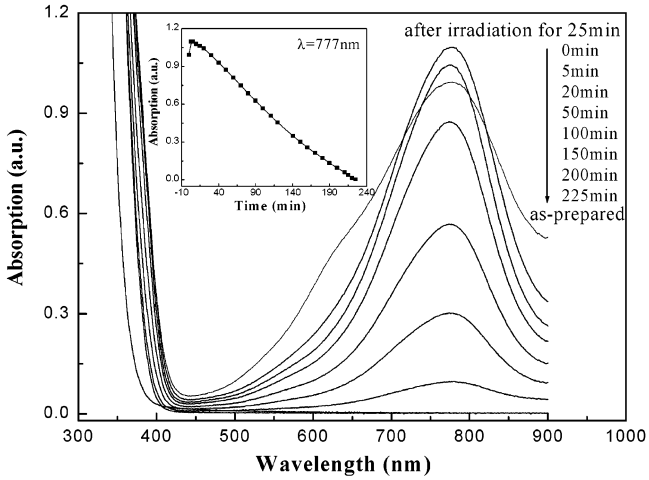

Figure 11. Absorption spectra on bleaching for sample A21 after UV-light irradiation for 25 min.

Figures 11 and 12 show the bleaching absorption spectra of samples A21 and B21 after being irradiated for 25 and 15 min, respectively. For comparison, the spectrum of the corresponding nonirradiated sample is also given. During the bleaching, the absorption peak at around 640 nm from $WOCl_x$ transforms to a peak at around 777 nm due to W^{5+} in the two samples. This transformation is caused by the hydrolysis of the $WOCl_x$ species and leads to longer lifetime W^{5+} state. Because $WOCl_x$ is unstable in aqueous solution and the amount of $WOCl_x$ in sample B21 is much larger than that in

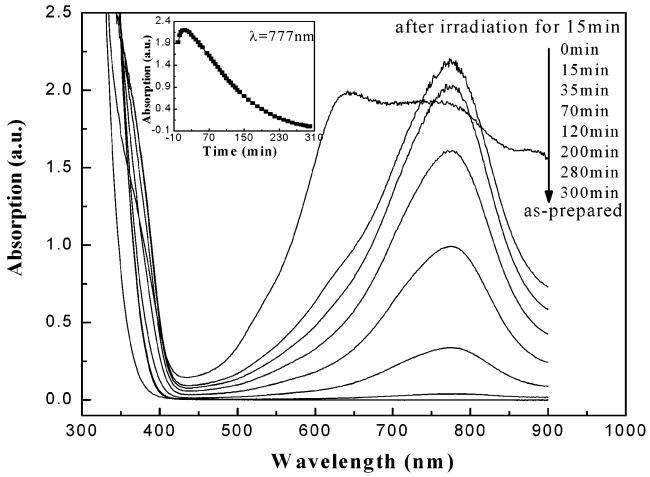

Figure 12. Absorption spectra on bleaching for sample B21 after UV-light irradiation for 15 min.

sample A21, it will take a longer time to reach the maximum absorption of W^{5+} for B21 than A21. This is confirmed by the fact that 15 min is needed for the former to reach maximum but only 5 min is needed for the latter. The bleaching rate, that is, the 777 nm band absorption as a function of resting time, is presented in the inset of Figures 11 and 12. The times for complete bleaching for sample A21 (225 min) and for B21 (300 min), are far longer than that of the colored WO_3 aqueous sol (no more than 30 min). From the absorption maximum of W^{5+}, the mean bleaching rates for B21and A21 are 7.72×10^{-3} /min and 4.98×10^{-3} /min, respectively. Apparently, the former bleaches faster than the latter, which is ascribed to the larger specific surface area and larger charge-transfer efficiency for smaller nanoclusters. In contrast to the absorption spectra of the nonirradiated samples, the band edges for the irradiated TiO_2-WO_3 mixed sols all redshift, due to both cluster growth and charge-transfer between TiO_2 and WO_3 during irradiation. Therefore, the charge-transfer between the WO_3 nanocluster and the TiO_2 nanocluster and the presence of the Cl^- ions cause the longer bleaching time for the mixed samples as compared with that of the WO_3 sol. Experimental results also indicate that large size is not good for WO_3 coloration because the re-irradiation of irradiated samples after color recovery produces lower coloration efficiency, so the aggregation and agglomeration may influence the coloration process at high concentrations, but are not an important factor.

Combining the TEM pictures with the absorption spectra of the nonirradiated separate and mixed samples, the band edge shift in the TiO_2-WO_3 mixed sol is related to the charge-transfer between the two nanoclusters, which may be the origin of the improvement of the photochromism of WO_3.

We have also tried to mix the TiO_2 sol obtained by hydrolysis of titanium ethoxide with WO_3 sol; however, the 640 nm band does not occur after UV light irradiation. Adding hydrochloric acid facilitates the appearance of this band, but the efficiency is low. This is believed to be due to the presence of the alcohol groups on the surface of TiO_2, which hinders the binding of the TiO_2 clusters with WO_3 and the charge-transfer between them.

Conclusion

The photochromic behavior of WO_3 nanoclusters is related to W^{5+} formation in the WO_3 nanoclusters. Under UV-light irradiation, an intrinsic absorption peak at around 777 nm from W^{5+} in the WO_3 sol appears, which generally appears at around 1000 nm in the WO_3 films, and shifts with cluster size due to the quantum confinement effect of delocalized carriers. Mixing WO_3 nanoclusters with TiO_2 nanoclusters leads to interfacial charge transfer. The TiO_2 nanoclusters can photocatalyze the formation and stabilization of W^{5+} in the WO_3 nanoclusters by the fast transfer of the photogenerated carriers between them. As a result, the chromic performance of the WO_3 aqueous sol is significantly improved by adding a TiO_2 sol. A size effect and the addition of Cl^- ions and TiO_2 nanoclusters also influence the phtotochromic behaviors of WO_3 sols. Moreover, a new extrinsic peak at around 640 nm appears in the mixed sols after adding TiO_2 nanoclusters. The formation of $WOCl_x$ species in the WO_3 sol, in the presence of Cl^- and TiO_2 nanoclusters, is assigned to this new peak. These results are important to the understanding of the chromism of tungsten oxides and their future applications.

Acknowledgment. We thank the National Natural Science Foundation of China under Grant 20173073 and Hundred Talents Projects of Chinese Academy of Sciences for the financial support.

CM034116G